Geoderma 430 (2023) 116290

Contents lists available at ScienceDirect

Geoderma

journal homepage: www.elsevier.com/locate/geoderma

Relevance of UAV and sentinel-2 data fusion for estimating topsoil organic carbon after forest fire

David Beltrán-Marcos [a,*], Susana Suárez-Seoane [b], José Manuel Fernández-Guisuraga [a,c], Víctor Fernández-García [a,d], Elena Marcos [a], Leonor Calvo [a]

[a] Area of Ecology, Department of Biodiversity and Environmental Management, Faculty of Biological and Environmental Sciences, University of León, 24071 León, Spain
[b] Research Institute of Biodiversity (IMIB; UO-CSIC-PA), Department of Organisms and Systems Biology (BOS; Ecology Unit), University of Oviedo, Mieres, Oviedo, Spain
[c] Centro de Investigação e de Tecnologias Agroambientais e Biológicas, Universidade de Trás-os-Montes e Alto Douro, 5000-801 Vila Real, Portugal
[d] Institute of Geography and Sustainability, Faculty of Geosciences and Environment, University of Lausanne, Geópolis CH-1015, Lausanne, Switzerland

ARTICLE INFO

Handling Editor: Morgan Cristine L.S.

Keywords:
Soil organic carbon
Image fusion
UAV
Sentinel-2
Wildfire
Soil properties

ABSTRACT

The evaluation at detailed spatial scale of soil status after severe fires may provide useful information on the recovery of burned forest ecosystems. Here, we aimed to assess the potential of combining multispectral imagery at different spectral and spatial resolutions to estimate soil indicators of burn severity. The study was conducted in a burned area located at the northwest of the Iberian Peninsula (Spain). One month after fire, we measured soil burn severity in the field using an adapted protocol of the Composite Burn Index (CBI). Then, we performed soil sampling to analyze three soil properties potentially indicatives of fire-induced changes: mean weight diameter (MWD), soil moisture content (SMC) and soil organic carbon (SOC). Additionally, we collected post-fire imagery from the Sentinel-2A MSI satellite sensor (10–20 m of spatial resolution), as well as from a Parrot Sequoia camera on board an unmanned aerial vehicle (UAV; 0.50 m of spatial resolution). A Gram-Schmidt (GS) image sharpening technique was used to increase the spatial resolution of Sentinel-2 bands and to fuse these data with UAV information. The performance of soil parameters as indicators of soil burn severity was determined trough a machine learning decision tree, and the relationship between soil indicators and reflectance values (UAV, Sentinel-2 and fused UAV-Sentinel-2 images) was analyzed by means of support vector machine (SVM) regression models. All the considered soil parameters decreased their value with burn severity, but soil moisture content, and, to a lesser extent, soil organic carbon discriminated at best among soil burn severity classes (accuracy = 91.18 %; Kappa = 0.82). The performance of reflectance values derived from the fused UAV-Sentinel-2 image to monitor the effects of wildfire on soil characteristics was outstanding, particularly for the case of soil organic carbon content (R^2 = 0.52; RPD = 1.47). This study highlights the advantages of combining satellite and UAV images to produce spatially and spectrally enhanced images, which may be relevant for estimating main impacts on soil properties in burned forest areas where emergency actions need to be applied.

1. Introduction

In recent years, the estimation of fire impact on ecosystems has become a challenge for forest managers in the Mediterranean Basin (Quintano et al., 2015), mainly because of the current increase in the extent and intensity of wildfires (Moreira et al., 2011). This fire regime shift, which has been attributed to fuel accumulation and continuity, as well as to increased drought events (Pausas and Fernández-Muñoz, 2012), may aggravate the ecological consequences of fire. In this sense, severe fires induce significant alterations in the structure and composition of vegetation and soil in forest ecosystems (Keeley, 2009), negatively affecting their capacity to provide ecosystem services (Calvo et al., 2015) and, particularly, their carbon storage function (Van Der Werf et al., 2010). Moreover, fire severity determines post-fire responses, severe fires deriving in poor plant regeneration, increased surface runoff, soil loss and flooding (Pausas et al., 2008; Pereira et al., 2018). In this context, it is particularly relevant to assess the ecological consequences of fire on forest soils in the short-term (Fernández-García et al., 2019a) in order to establish management and restoration post-fire actions in highly vulnerable areas. Soil burn severity is a commonly-used

* Corresponding author.
E-mail address: dbelm@unileon.es (D. Beltrán-Marcos).

https://doi.org/10.1016/j.geoderma.2022.116290
Received 24 August 2022; Received in revised form 3 November 2022; Accepted 25 November 2022
Available online 2 December 2022

term to describe fire-induced changes in organic and mineral soil layers (Neary et al., 2005; Lentile et al., 2006), including physical and chemical properties (i.e., organic matter content, aggregate stability, water repellence, moisture or pH) and microbiological or biochemical properties (i.e., microbial biomass, microbial activity or soil enzymatic activities; Vega et al., 2013; Fernández-García et al., 2019a). The consequences of fire severity on soil properties have been evidenced in many studies, describing minimal effects at low severity, with even positive effects on some soil properties (Alcañiz et al., 2018), such as an appreciable value profit of soil organic carbon (Marcos et al., 2009) caused by the incomplete combustion of the litter layer. A similar effect has been found for mean weight diameter of soil aggregates (Marcos et al., 2018). At low burn severity, fire does not produce noticeable changes on the aggregate size classes. However, as a result of the increase in organic matter with cementing action at low temperatures (Mataix-Solera et al., 2002), a slight increase in the coarse fraction aggregates (>1–2 mm) has been found (Mataix-Solera et al., 2011). Conversely, pronounced effects are associated with high soil burn severity levels, with a significant decrease of mean aggregate size (Marcos et al., 2009; Marcos et al., 2018). The high temperature reached at the first five centimetres of soil lead to important quantitative and qualitative transformations of the organic matter, whereas water absorption and retention, porosity and infiltration capacity are considerably reduced (Mataix-Solera et al., 2011). In-depth knowledge on soil attributes useful as indicators of fire-induced ecological changes remains a challenge for post-fire land management and restoration actions.

Although there is no unique approach to measure burn severity (Keeley, 2009), the scientific community usually employs the Composite Burn Index (CBI) for a ground-based assessment of the magnitude of ecosystem changes caused by fire (Key and Benson, 2006; Keeley, 2009). Based on visually estimated metrics, the CBI procedure assesses the impact of fire on vegetation (vegetation burn severity) and soil (soil burn severity), either jointly or separately, depending on the ecosystem compartments wanted to be considered (Key and Benson, 2006; Keeley, 2009). Nevertheless, since large wildfires often produce mixed severity land mosaics (Vega et al., 2013), traditional sampling methods alone are no longer considered suitable to explore soil damage at large-scale due to cost-effectiveness and lack of spatial exhaustiveness (Morgan et al., 2001). This is especially noticeable when the spatial patterns of burn severity are highly variable (Johnstone and Chapin, 2006). Remote sensing techniques, including satellite and aerial imagery, provide new tools for retrieving information on fire impacts across large areas in a variety of scales quickly and at a low economic cost (Lentile et al., 2006). Based on the energy-matter interaction principles, spectral data across the visible, near infrared and shortwave infrared (VIS, NIR and SWIR, respectively) regions are able to provide qualitative and quantitative information on soil status. The combination of data from different spectral regions further allow the estimation of a wide array of spectral indices, such as the Normalized Burn Ratio (NBR), that is sensitive to the vegetation influence on some topsoil properties, such as soil organic carbon (SOC) content (Castaldi et al., 2019a). Great advances have been made in the characterization of soil properties from multispectral data, but no single sensor type or data analysis method has already been reported as the best for monitoring a particular soil property (Ge et al., 2011). For example, a few studies have detailed the potential of Sentinel-2 (spatial resolution of 20 m) and Landsat-8 (spatial resolution of 30 m) satellite imagery for predicting and mapping soil properties (Castaldi et al., 2016; Gholizadeh et al., 2018; Žížala et al., 2019). Indeed, Sentinel-2 imagery was used with promising results for SOC estimation in croplands at a regional scale, where the spatial resolution and spectral characteristics of this sensor were adequate to describe the soil spatial variability (Castaldi et al., 2019b; Vaudour et al., 2019). Notwithstanding, this medium spatial resolution could be insufficient to explain the high spatial variability that characterizes soil properties across burned forest ecosystems. Therefore, there is a gap in the development of tools that provide accurate spatial information of fire effects on physical and biochemical soil parameters at fine spatial scale in forest ecosystems.

In this sense, unmanned aerial vehicles (UAV) provide very high spatial resolution imagery (higher than 1 m), at relatively low cost (Aldana-Jague et al., 2016), which may be used to evaluate the impact of fire on soil properties in heterogeneous burned areas, particularly where high spatial accuracy is required (Fernández-Guisuraga et al., 2018). Nonetheless, research concerning soil property estimation with UAVs is limited due to the insufficient spectral resolution of the available multispectral sensors (Zhang and Kovacs, 2012). In general, UAV multispectral sensors only collect data across visible (VIS) and near-infrared (NIR) regions (Aldana-Jague et al., 2016), which is a handicap considering that the most fundamental spectral signatures of soil components appear in the mid-infrared (MIR) and thermal- infrared wave ranges (Soriano-Disla et al., 2017). Moreover, most UAV remote sensing advances have been made under fairly controlled conditions in homogeneous environments, such as croplands (Crucil et al., 2019). Nevertheless, to our knowledge, there are no studies applying this technology to the evaluation of changes in soil properties at fine spatial scale after significant disturbances, such as a forest fires.

Among the approaches that may serve to resolve limited UAV spectral resolution, image sharpening techniques to fuse remote sensing images are a potential alternative (Laben and Brower, 2000; Ehlers, 2004). The image sharpening technique is based on the combination of spectral characteristics of images with different spatial resolution to generate spatially improved images (Yilmaz and Gungor, 2016). This fusion technique uses a fine band from the highest spatial resolution image as a reference, which is combined with the spectral bands of the image at lower spatial resolution, generating a new multiband image that preserves the highest spatial and spectral resolution. On this subject, recent advances in the fusion methods have been developed, employing satellite (Landsat 8 OLI MS, Sentinel-2A MSI, WorldView-2) and UAV images data in agricultural applications (Jenerowicz and Woroszkiewicz, 2016; Yilmaz and Gungor, 2016; Zhao et al., 2019). However, there use of this technique in burned areas with successful results remains as a challenge.

Based on the research gaps found in the literature, the main purpose of this study is to assess the potential of fusing multispectral images with different spectral and spatial resolutions to estimate soil properties sensitive to fire-induced changes. To this end, we determined post-fire effects on soil by burn severity, and assessed whether soil moisture content (SMC), soil organic carbon (SOC) and aggregate stability measured as mean weight diameter (MWD) can perform as useful indicators of soil burn severity. Next, we analyzed the ability of multispectral images with different spectral and spatial resolutions (UAV, Sentinel-2 and fused UAV-Sentinel-2) to predict the soil properties more suitable to discriminate soil burn severity. According to other authors who consider that the spatial resolution has a lower effect than the spectral resolution on the prediction of soil properties (Žížala et al., 2019), we expect that images with low-spectral and high-spatial resolution (UAV data) would have less predictive capacity than those with higher spectral and lower spatial resolution (Sentinel-2 data). Moreover, we hypothesized that the fusion of images with different spatial and spectral resolutions (UAV and Sentinel-2 data) would improve the predictive capacity of soil properties, compared with UAV or Sentinel-2 individual images. Finally, we examined which spectral bands were the most important predictors of fire impact on soil properties.

2. Materials and methods

The experimental design defined for this study is summarized in the methodological flowchart shown in Fig. 1.

2.1. Study site description

The study site is located within the perimeter of a stand-replacing fire

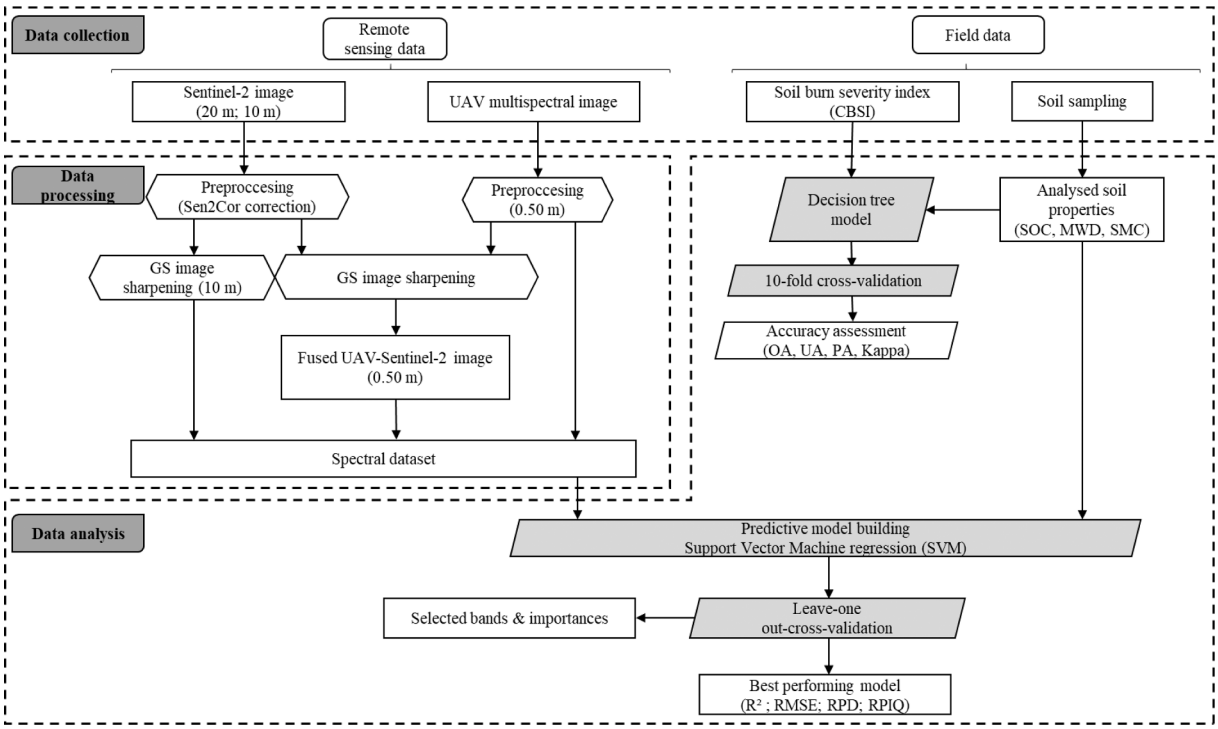

Fig. 1. Research methodology flowchart used in this study (UAV: unmanned aerial vehicle; CBSI: Composite Burn Soil Index; GS: Gram–Schmidt transformation; SOC: soil organic carbon; MWD: mean weight diameter; SMC: soil moisture content; OA: overall accuracy; UA: useŕs accuracy; PA: produceŕs accuracy; SVM: support vector machine; RMSE: root-mean-square error).

that occurred on 22nd August 2019 and burned 82.47 ha of a complex landscape mosaic. The study was conducted on an east-facing hillside of Villapadierna (Cantabrian mountain range, NW Spain; Fig. 2A), where the dominant vegetation types are: (i) extensive mature forest stands of *Quercus pyrenaica* Willd. with a dense shrubby understory of heaths of *Erica australis* L. and *Erica arborea* L. and gorse of *Halimium alyssoides* Lam., and (ii) pine forest plantations of *Pinus sylvestris* L. and *Pinus pinaster* Ait. The area affected by the fire presents a smooth orography, with elevation ranging from 922 to 1027 m.a.s.l. and slopes from 6 to 27 %. Soils are classified as Dystric, Gleyic and Humic Cambisols (ITACYL, 2020), according to the World Reference Base for Soil Resources (WRB) system (Jones et al. 2005). The dominant lithological material is composed by silts, sands and clays, with conglomerate layers in the lowest areas (GEODE, 2019; Beltrán-Marcos et al., 2021). The soil parent material is characterized by slight or moderate weathering, and by the absence of appreciable quantities of illuviated clay and organic matter, mainly in the lowest zones. Soil texture is sandy-loam. Climate is Mediterranean with an annual average precipitation of 761 mm, a mean annual temperature of 10.7 °C and 2–3 months of summer drought (Ninyerola et al., 2005).

2.2. Field data and soil sampling

One month after the wildfire, we estimated in the field soil burn severity using 34 plots of 50 cm × 50 cm. Field plots were randomly distributed within homogeneous 2 m × 2 m soil burn patches situated in areas without tree canopy to avoid interference in the UAV and Sentinel-2 imagery acquisition (Fig. 2A). A minimum distance between plots of 25 m was ensured. All plots were located in a study framework of 16 ha that was representative of all scenarios of burn severity occurred within the fire perimeter. The study framework presented a fairly uniform topography with an average slope of 10.41 %±3.02 % over a Humic Cambisol - Gleyic Cambisol soil association (ITACYL, 2020). The plots were georeferenced by means of a sub-meter accuracy GNSS receiver in postprocessing mode.

In each plot, we estimated visually soil burn severity using a Composite Burn Soil Index protocol (CBSI) proposed by Beltrán-Marcos et al. (2021) (Table 1). The CBSI is an adaptation of the substrate stratum of the original and widely used Composite Burn Index (CBI; Key and Benson, 2006). Soil burn severity was classified (Parks et al., 2014) as unburned (0), low-moderate severity (0.1–2.24) and high severity (2.25–3), according to the values estimated visually for the rating factors indicated in Table 1. Several studies (e.g., Miller and Thode, 2007; Quintano et al., 2015) proposed to differentiate the high severity level from the rest of the burn severity classes to accurately discern burn severity in remote sensing-based approaches (Fig. 3).

To analyze the relationships between soil burn severity and soil properties, we collected one soil sample from each 50 cm × 50 cm plot, made of a mix of four random subsamples. Each subsample corresponded to the volume of a core of 5 cm diameter × 3 cm depth and was collected after removing litter, woody and fine debris from the surface. Half of the sample was air-dried immediately after sampling and stored at 20 °C until laboratory analysis. The rest of the sample was transported to the laboratory for analysis in cooler insulated containers and stored at − 18 °C until laboratory analysis. There was no precipitation or external interference within seven days before field sampling to ensure the objectivity and reliability of the data.

2.3. Soil analysis procedures

In each soil sample, the following biophysical properties were analyzed: mean weight diameter (MWD), soil moisture content (SMC) and soil organic carbon (SOC). MWD was determined by dry screening of soil aggregates (Kemper and Rosenau, 1986). Dry soil samples were sieved during two minutes through 2, 1, 0.25, 0.1- and 0.05-mm sieves in an electromechanical shaker. The percentage of aggregates was calculated for each fraction through the ratio between the amount of aggregate retained on each sieve and the total amount of sample analyzed. These results allowed to calculate the mean weight diameter (MWD) using the following equation (Eq. (1)):

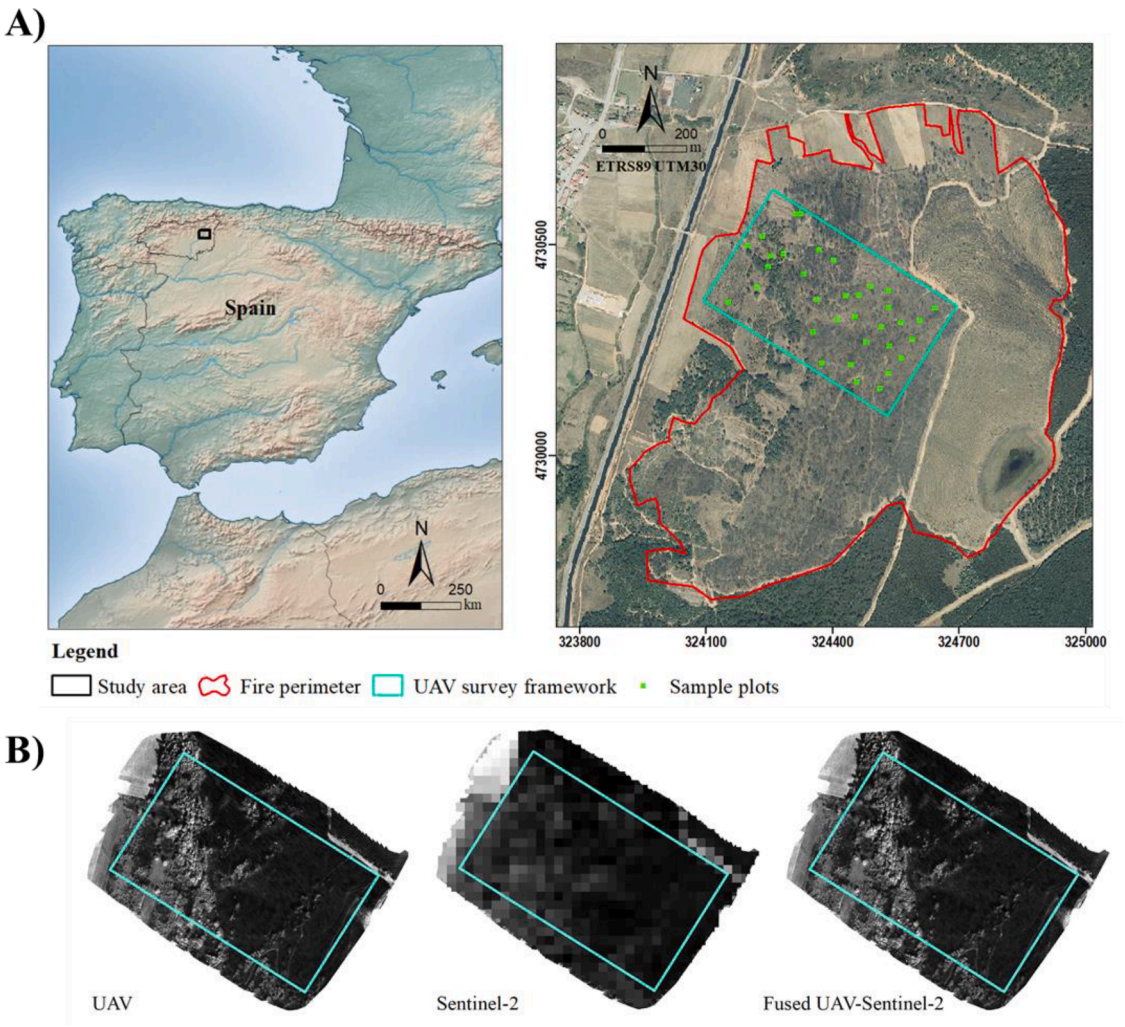

Fig. 2. A) Location of the study area in the NW of the Iberian Peninsula (Spain) and the spatial distribution of field plots in the study framework of 16 ha established within the fire perimeter. B) UAV, Sentinel-2 and fused UAV-Sentinel-2 orthomosaics in the NIR band (wavelength range 785–900 nm).

Table 1
Composite Burn Soil Index (CBSI) factors and scores used to obtain field values of soil burn severity (based on Key and Benson, 2006).

Strata Rating Factors	Soil burn severity scale						
	Unburned	Low		Moderate		High	
	0	0.5	1	1.5	2	2.5	3
Litter/light fuel consumed	None	<10 %	10–20 %	20–40 %	40–80 %	80–98 %	98 %
Medium/heavy fuel consumed	None		20 % consumed		40 % consumed		>60 % consumed
Ash colour	None	Blackened litter, no changes in soil		Charred remains, recognizable litter		Grey and white ash, grey soil	White ash, reddened soil
Char depth	None	<1 cm		1–3 cm		>3 cm	

$$MWD = \sum_{i=1}^{n} X_i W_i \quad (1)$$

where X_i is the mean diameter of the size classes (mm) and W_i is the weight of each soil fraction (%).

SMC was determined gravimetrically after drying a known amount of fresh subsample soil to a constant weight at 105 °C over 24-h and results were expressed as the water percentage in dry soil. SOC was analyzed by grinding the soils to 0.15-mm particle size employing a pestle and mortar and applying Walkley–Black dichromate digestion (Nelson and Sommers, 1982).

2.4. Remotely sensed data and processing

Multispectral data from Sentinel-2 MSI, Parrot Sequoia camera on board a UAV platform and fused UAV-Sentinel-2 datasets (Fig. 2B) were used to predict biophysical soil properties after fire. The main technical specifications of the multispectral sensors and acquisition dates are summarized in Table 2. Acquisition times of multispectral imagery were selected as close as possible to the field sampling period to minimize the effect of unwanted changes in the soil surface conditions. No significant precipitation was recorded between both field work and remote sensed data acquisition dates.

2.4.1 Sentinel-2 dataset

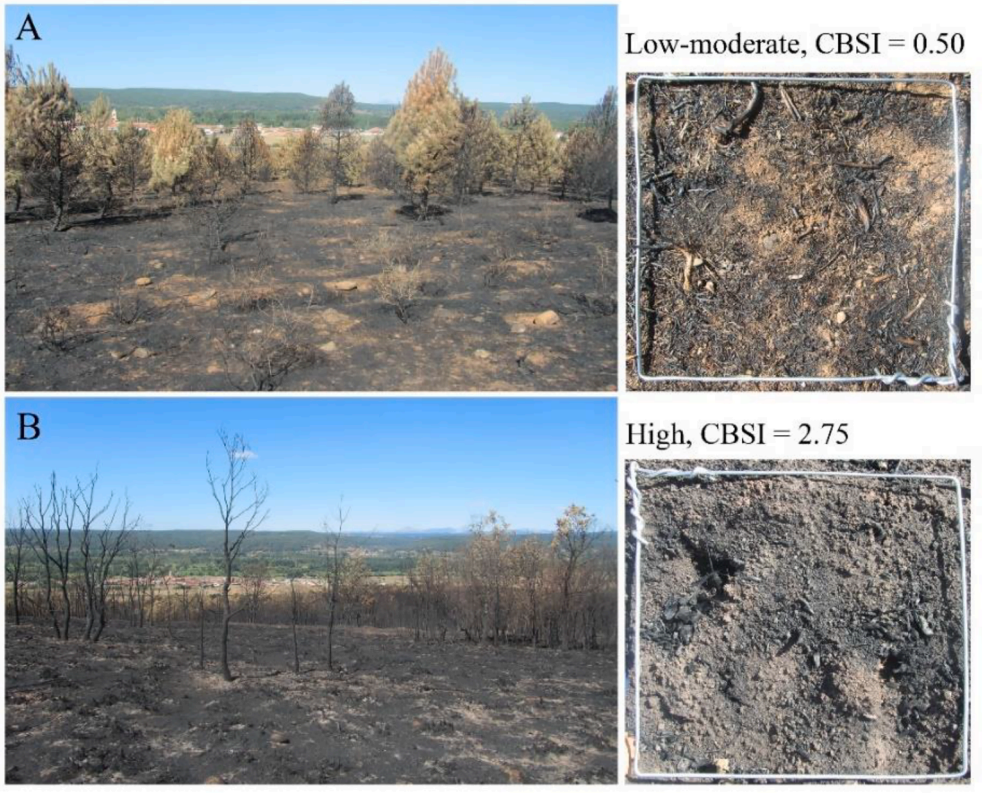

Fig. 3. Scenarios of soil burn severity considered in this study. CBSI: Composite Burn Soil Index.

Table 2
Main technical characteristics of the multispectral sensors considered in this study. MSI: Multispectral instrument; UAV: unmanned aerial vehicle; NIR: Near-infrared; FWHM: Full width at half maximum; GSD: Ground sampling distance.

Sensors	Mission	Sensor type	Spectral bands	Used spectral bands	Central wavelength (nm)	FWHM (nm)	GSD (spatial resolution)	Acquisition date
Sentinel-2A (ESA, 2021)	Spaceborne	Pushbroom scanner	13	BLUE (B2)	492	66	10 *m*	29–09-2019
				GREEN (B3)	560	36	10 *m*	
				RED (B4)	665	31	10 *m*	
				RED-EDGE-1 (B5)	704	15	20 *m*	
				RED-EDGE-2 (B6)	741	15	20 *m*	
				RED-EDGE-3 (B7)	783	20	20 *m*	
				NIR (B8)	833	106	10 *m*	
				NIR narrow (B8A)	865	21	20 *m*	
				SWIR-1 (B11)	1614	91	20 *m*	
				SWIR-2 (B12)	2202	175	20 *m*	
Parrot Sequoia	UAV	4 × 1.2 Mpix Global shutter frame sensors	4	GREEN (B1)	550	40	5.6 cm	25–09-2019
				RED (B2)	660	40		
				RED-EDGE (B3)	735	10		
				NIR (B4)	790	40		

A cloud-free Sentinel-2A Level 1C image covering the study framework was downloaded from the European Space Agency's (ESA) Copernicus Open Access Hub platform (). This scene was topographically and atmospherically corrected to obtain a Sentinel-2 Level 2A product (ESA, 2018). The Sen2Cor algorithm implemented in Sentinel Application Platform (SNAP) 7.0 version and a digital terrain model (DTM) with a grid of 25 m (https://centrodedescargas.cnig.es/) were used for this purpose. Sentinel-2 provides spectral data over the visible (VIS), near infrared (NIR) and shortwave infrared (SWIR) regions. Each Sentinel-2 image is composed by 13 spectral bands with different spatial resolutions: three bands at 60 m, six bands at 20 m and four bands at 10 m (Table 2). The 60 m bands (B1, B9 and B10) are primarily used to perform atmospheric and radiometric corrections (cirrus detection and estimation of water vapor content) (ESA, 2021). Moreover, scattering of radiation by the gases and aerosols significantly influences the reflectance in these bands (Jia et al., 2016), causing inappropriate surface reflectance measures (Rivera et al., 2013). Consequently, they were discarded for further analysis.

2.4.2 UAV multispectral dataset

An FV8 octocopter developed by ATyges (ATyges Ingeniería, Málaga, Spain, Fig. 4), equipped with a Parrot Sequoia sensor, was also used for multispectral imagery acquisition covering the sampling framework. Through a global shutter with four monochrome sensors and a resolution of 1.2 megapixels, the Parrot Sequoia camera allows to acquire images along four discrete bands in the visible (green, red and red-edge) and near-infrared (NIR) spectral regions (Table 2). On 25th September 2019, between 11:00 and 13:00 UTC, we carried out six UAV flights at a height of 50 m above ground level to capture multispectral imagery in optimal atmospheric conditions in terms of lighting and wind. Radiometric calibration for each flight was performed using a target calibration in order to obtain absolute reflectance values. The Parrot Sequoia camera works in combination with an incident light sensor that provides an image-level correction factor for adjusting illumination conditions during image acquisition. The camera trigger interval and the waypoint route planned allowed the collection of 5060 georeferenced multispectral images with an 80 % front and 80 % side overlap, with an average ground sample distance (GSD) of approximately 5.6 cm.

The photogrammetric processing of the imagery was carried out using AgiSoft PhotoScan Professional 1.2.6 (AgiSoft LLC, St. Petersburg, Russia). This software integrates computer vision techniques and photogrammetry algorithms based on the works of Puliti et al. (2015) and Ruzgiene et al. (2015) to obtain high-accuracy orthoimages. Moreover, it includes the Sequoia camera model to extract automatically relevant information about camera, calibration panels and sun sensors directly from EXIF files, where all image metadata is stored. The application of structure-from-motion (SfM) algorithms enabled the computation of dense 3D point clouds to generate a digital elevation model (DEM) and a multispectral orthomosaic with four radiometric bands. The orthomosaic was georeferenced using 16 ground control points (GCP) to obtain a root-mean-square error in X, Y (RMSExy) < 3 cm and 3 cm in Z. Finally, the multispectral orthomosaic was resampled to 0.50 m of spatial resolution using the bilinear interpolation technique. Reflectance values were extracted for each field plot by averaging the values of a grid of 20 points systematically distributed within each 50 cm $\times$ 50 cm plot, with a spacing distance between points fixed at 10 cm.

2.4.3 Data fusion

Sentinel-2 images were sharpened using ENVI 5.3 software (Exelis Visual Information Solutions) following a Component Substitution (CS) approach, which substitutes a high-resolution image by the selected band after spectral transformation (Vivone et al., 2015), and a Gram-Schmidt (GS) transformation algorithm (Laben and Brower, 2000). The GS algorithm transforms a multidimensional image by applying an orthogonal transformation, which produce a new set of orthogonal and linear independent bands (Laben and Brower, 2000). It is one of the most widely used methods of image fusion (Maurer, 2013), since: (i) it is capable of sharpening more than three spectral bands; (ii) it preserves the quality of the multispectral information well, attenuating spectral distortions (Zhang and Mishra, 2012); and, (iii) it is faster and less computationally complex than other similar methods (Jenerowicz and Woroszkiewicz, 2016; Zhao et al., 2019; Jones et al., 2020). First, it generates a simulated low-resolution panchromatic band that must fall in the spectral range of the high spatial resolution or fine band (Laben and Brower, 2000), through a weighted linear combination of multispectral low spatial resolution bands. Second, GS orthogonalization is performed on all bands, setting the simulated panchromatic band as the first band. Third, an inverse Gram-Schmidt transformation is applied to produce the spatially enhanced image (Laben and Brower, 2000; Ehlers et al., 2010).

The band selection scheme has proven to be the most reliable and straightforward approach for spatial information enhancement through CS (Kaplan, 2018), and ensuring that the simulated band and the reference fine band are within the same spectral range is essential for a better preservation of the spectral characteristics (Laben and Brower, 2000). To sharpen the six bands of Sentinel-2 at 20 m to 10 m spatial resolution, the near-infrared band (B8) from the higher spatial resolution image was used as fine band. This band was the closest spectral candidate during image sharpening and had significant spectral sensitivity with SWIR bands, as demonstrated in other studies (Vaiopoulos and Karantzalos, 2016). The near-infrared narrow band (B8A) was used as the simulated first band of the low-resolution multispectral data input of the GS transformation owing to their spectral correspondence with B8 (Kaplan, 2018). For the case of the fusion between 20 m Sentinel-2 and 0.50 m UAV bands, the fine band was the near-infrared band (B4) of the UAV high spatial resolution image, according to a spectral proximity range criterion (Laben and Brower, 2000; Vaiopoulos and Karantzalos, 2016). In the same way, the UAV red band (B2) was used as the fine band to sharpen the 10 m Sentinel-2 bands up to 0.50 m. The Sentinel-2 red-edge 3 band (B7) at 20 m and the Sentinel-2 red band (B4) at 10 m were employed as simulated lower resolution panchromatic bands and performed as the first band in separated GS transformations. The selection of Sentinel-2 NIR band (B8) at 10 m was discarded for presenting a dissimilar spectral response with respect to the UAV bands. Previous studies have demonstrated the effectiveness of the GS algorithm in compensating for large spatial resolution differences, e.g. between multispectral images acquired by UAVs and satellite platforms (Jenerowicz and Woroszkiewicz, 2016; Zhao et al., 2019).

The quality measurement of the fused image was evaluated using the ERGAS (Erreur Relative Globale Adimensionalle de Synthèse) index proposed by Wald et al. (1997). This index describes the overall error of a fused image according to the independence of the spectral bands under consideration and independence of the spatial resolutions. The smaller ERGAS value, the higher the spectral quality of the fusion (Alparone et al., 2007). Fig. 5 displays a general overview of the image fusion

Fig. 4. ATyges FV8 octocopter used in this study to collect UAV multispectral imagery. The red frame indicates the position of the multispectral Parrot Sequoia camera. (For interpretation of the references to colour in this figure legend, the reader is referred to the web version of this article.)

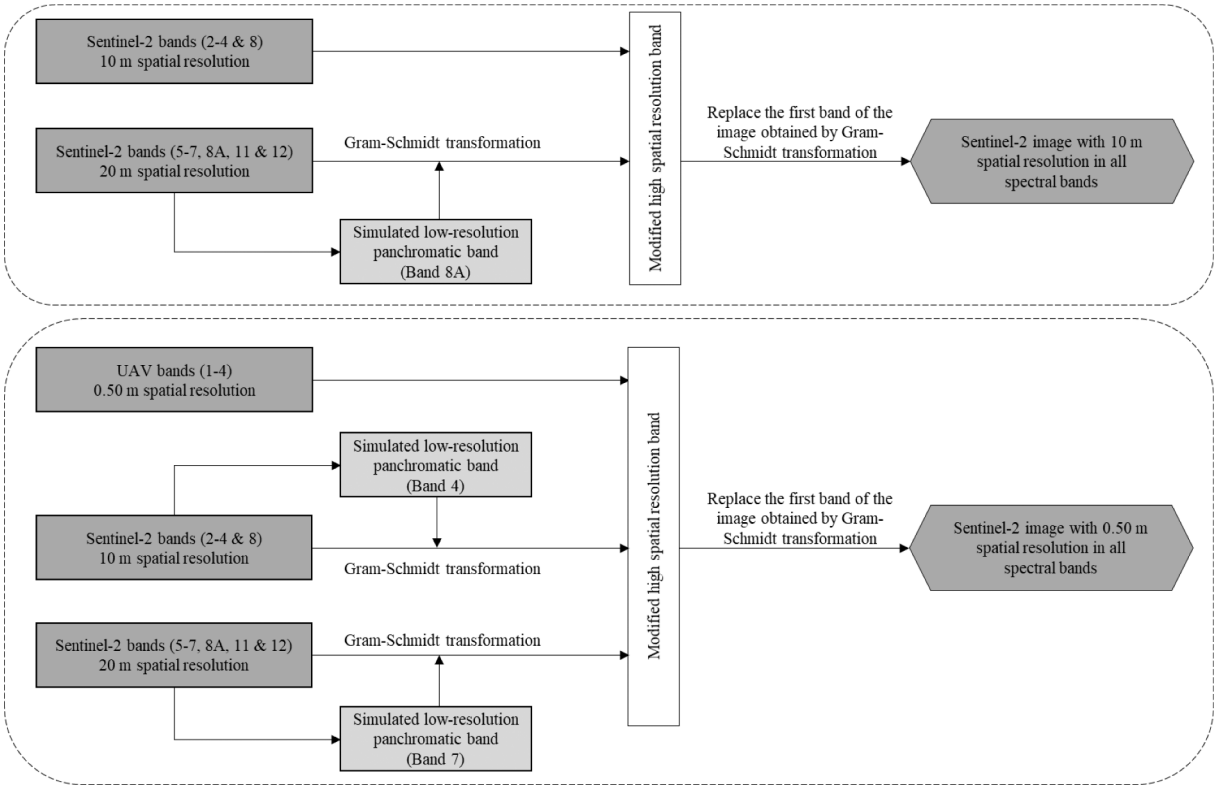

Fig. 5. The process of Gram-Schmidt (GS) transformation to produce spatially enhanced images from UAV and Sentinel-2 products.

methodology. Finally, the fused UAV-Sentinel-2 dataset, as well as the UAV and Sentinel-2 datasets were used to predict post-fire soil properties in the field plots. We also computed two spectral indices (the normalized difference vegetation index -NDVI- and the normalized difference water index -NDWI-) widely used in the literature for their high sensitivity to soil burn severity (Beltrán-Marcos et al., 2021), and based on the availability of common bands in the three datasets, to predict the spatial variation of the CBSI in the study site.

2.5. Statistical analyses

A decision tree (DT) classifier was used to determine which soil properties (SOC, MWD and SMC) were more related to soil burn severity in the full soil sample dataset. This hierarchical machine learning technique allowed to model the relationship among the response variable (soil burn severity) and explanatory variables (soil properties) without any assumption about the distribution of data (Tehrany et al., 2013). DT was calibrated using 10-fold cross-validation resampling technique, which has proven to yield reliable results without requirement of an independent dataset to evaluate the model accuracy (Sherrod, 2008). DT was constructed by repeatedly dividing the dataset into homogeneous classes based on the response variable (Collins et al., 2007). DT produces a collection of nodes based on the most characteristic soil properties values where entropy was used to measure the uncertainty of each decision. This process is repeated until either a minimum subset size is reached, holding the most information about the categorical dependent variable (soil burn severity). This tool allows to handle non-linear or discontinuous relationships between variables, offering advantages over traditional classification algorithms (De'ath and Fabricius, 2000) and showing easily interpretable data outputs. In addition, we used an optimal complexity parameter (cp) to achieve the highest performance in DT classifier (Breiman et al., 2017). DT model outputs were assessed through their overall accuracy (OA), producer's accuracy, user's accuracy and Kappa coefficient.

We implemented a Support Vector Machine (SVM) algorithm to predict SOC, SMC and MWD from Sentinel-2, UAV and fused UAV-Sentinel-2 datasets. Due to the limited number of soil samples available, a leave-one-out cross-validation (LOOCV) procedure was used to test the prediction capacity of the SVM models for the entire dataset and avoid over-fitting (Lu et al., 2013). This method uses $n - 1$ samples to calibrate the model, leaving the excluded sample for validation purposes. This process was iteratively repeated for all n samples. SVM is one of the most widely applied machine learning methods to estimate soil parameters (e.g. Aldana-Jague et al., 2016; Žížala et al., 2019). It minimizes overfitting and produces reliable results with small datasets (e.g. < 100 samples) (Genuer et al., 2010; Stevens et al., 2012; Debaene et al., 2014; Kisi and Parmar, 2016). It uses a linear model based on statistical learning to resolve non-linear discrimination in classification, regression, mapping or other tasks in a high-dimensional feature space defined by a kernel function (Vapnik, 1995). In this study, we chose the radial basis kernel function, as it has been successfully used in other studies of fire ecology based on remote sensing data (Dragozi et al., 2014). SVM-models were optimized using a grid search method which determines the best parameters in each prediction. Cost (C) and kernel function (g) parameters were also tuned through LOOCV to maximize model accuracy. The SVM algorithm was also used to model the relationship between CBSI field-measured and CBSI-estimated values by NDVI and NDWI spectral indices in each multispectral dataset.

The coefficient of determination (R^2) was used to evaluate model accuracy, whereas the root-mean-square-error (RMSE) was quantified as a measure of predictive performance. Moreover, predictive performance was also assessed using the ratio of predicted deviation (RPD) and the ratio of performance to interquartile range (RPIQ). Both statistics properly describe the range of variation of the data and are considered reliable for describing the model performance that follow a non-normal distribution (Shi et al., 2020). In order to detect the spectral regions with higher predictive capacity of soil properties, we provided the relative importance of the spectral bands used to SVM calibration. We applied a global sensitivity analysis (GSA), which explores the effects of each combination of input variables on the assigned output response (Cheng

et al., 2017). A Kruskal-Wallis test, with a significance of 5 %, was applied to evaluate differences among spectral bands. All statistical analyses were conducted in R software (R Core Team, 2019) using the packages "tree" (Ripley, 2019), "MASS" (Venables and Ripley, 2002), "rpart" (Ripley et al., 2022), "caret" (Kuhn, 2008), "rminer" (Cortez, 2020) and "e1071" (Meyer et al., 2015).

3. Results

3.1. Effects of burn severity on soil properties

Soil biophysical properties varied widely across the study site, with particular relevance for SMC (coefficient of variation -CV- = 77.31 %). The value of all soil parameters always decreased with burn severity. Nevertheless, the magnitude of the fire impact differed notably across them (Table 3). SOC values accounted in plots burned at low-moderate burn severity were lower than those accounted in plots affected by high burn severity. MWD of soil aggregates diminished slightly with severity, while SMC values were more strongly affected.

3.2. Soil burn severity discrimination through soil properties

Decision tree (DT) analysis featured a high performance to classify soil burn severity through the considered soil properties (overall accuracy and Kappa of 91.18 % and 0.82, respectively). DT was composed of seven nodes, where each node established a splitting rule according to the values of the most important soil biophysical parameters to classify burn severity (Fig. 6). These splitting rules and their uncertainty are described in Table SM1 in supplementary material. DT classification model featured a high specificity for classifying high burn severity samples (produceŕs accuracy -PA- = 100 %). Further details of computed confusion matrix are presented in Table SM2 in supplementary material. DT output showed that SMC and SOC were the best indicators of soil burn severity. SMC was set as the first node, with values lower than 1.9 % indicating high soil burn severity. Likewise, SOC was included in the second node of the classification, with values higher than 48 μg C/g, corresponding to low-moderate burn severity, and values between 36 and 48 μg C/g dry soil, indicating a high burn severity.

3.3. Spectral reflectance of soil samples

The mean spectral reflectance of the field plots was similar for the three considered spectral datasets (Sentinel-2, UAV and fused UAV-Sentinel-2) across the VIS-NIR (400–900 nm) spectral region (Fig. 7). Nonetheless, significant differences were found in the NIR region (above 700 nm) for UAV data with respect to the other datasets (Kruskal-Wallis test, $\chi^2 = 6.51$; p-value < 0.05), with the highest reflectance values being captured by the Parrot Sequoia camera. In the NIR-SWIR (900–2350 nm) spectral region, mean reflectance values of fused spectral signature had a similar trend than Sentinel-2 spectral signature, as found for the VIS-NIR, which indicates remarkable spectral consistency in all absorption bands related to soil characteristics. The ERGAS value of 0.130 also indicates a high degree of similarity between the original image and the fused image, i.e. a high level of spectral information preservation. The spectral signatures of each soil burn severity level were compared to obtain a better understanding of their spectral behaviour and potential discriminatory ability. The near-infrared region (NIR) (700–900 nm) offered greater discrimination than the visible one (400–690 nm) for all spectral dataset, and the lowest spectral distance was obtained in SWIR bands where severely burned areas began to show higher reflectance (see Figure SM1 and SM2 in supplementary material for further details on spectral signatures). The relationship between CBSI field-measured and CBSI-estimated values by NDVI and NDWI spectral indices computed from the fused UAV-Sentinel-2 dataset featured a higher performance than the computed from Sentinel-2 and UAV images (Table SM3 and Figure SM3 in supplementary material.

3.4. Prediction of SOC and SMC from spectral data

The predictive performance varied according to the spectral dataset used (Table 4). Sentinel-2 at 10 m of spatial resolution was the spectral dataset that produced the SOC models with the weakest accuracy and predictive performance (R^2 = 0.13, RPD = 0.96). Nevertheless, this dataset featured the best SMC models (R^2 = 0.11, RMSE = 1.93, RPD = 1.05) (Table 4). When using the UAV spectral dataset at 0.50 m as predictor of SOC content model evaluation improved notably (R^2 = 0.24, RPD = 1.14). Indeed, training the models with fused UAV-Sentinel-2 data had a much better performance (R^2 = 0.52, RMSE = 7.83, RPD = 1.47) (Fig. 8). However, in the case of SMC, UAV and fused data did not perform well.

In the case of UAV data, green (B1) and near-infrared (B4) spectral bands (wavelengths ranging between 510 and 590 and 750–830 nm, respectively) were of the greatest importance for the evaluation of soil properties through GSA analysis, especially for the case of SOC (Fig. 9). Regarding Sentinel-2 data, both visible and SWIR bands (492–665 nm and 1614–2202 nm wavelength, respectively) were the most important, particularly for SMC. As for the fused data, wavelengths belonging to the SWIR (1614–2202 nm) and visible (492–665 nm) regions of the spectrum were significantly useful for estimating SOC.

4. Discussion

The results of this study evidenced the suitability of remote sensing fusion techniques of images with high spatial and spectral resolution to predict soil properties in a Mediterranean forest landscape affected by fire, with particularly good results for SOC, which is one of the best soil indicators of burn severity. This result, that is in line with previous studies (Mataix-Solera et al., 2002; Badía et al., 2017; Fernández-García

Table 3
Descriptive statistics for the soil properties affected by fire in the study area: soil organic carbon (SOC), mean weight diameter (MWD) and soil moisture content (SMC). Columns report basic statistics including the number of samples (n), minimum values (Min), maximum values (Max), mean values (Mean), Q1 – First quartile, Q3 – Third quartile, standard deviation (SD), coefficient of variation (CV) and coefficient of skewness (Skew).

Soil properties	Soil burn severity scenario	Min	Q1	Mean	Q3	Max	SD	CV	Skew
SOC (μg C·g − 1 soil)	Overall	21.72	33.76	41.38	47.30	75.74	11.47	27.30	0.99
	Low-moderate	26.40	33.36	44.43	52.25	75.74	14.60	32.87	0.72
	High	21.72	36.10	38.67	42.95	47.60	7.14	18.46	−0.90
MWD (mm)	Overall	0.63	0.76	0.95	1.07	1.30	0.19	20.55	0.28
	Low-moderate	0.63	0.75	0.97	1.12	1.30	0.23	23.27	0.01
	High	0.70	0.79	0.93	1.04	1.26	0.17	17.87	0.53
SMC (%)	Overall	0.85	1.52	2.62	2.85	9.85	2.03	77.31	2.72
	Low-moderate	1.36	2.20	3.56	3.73	9.85	2.58	72.45	1.94
	High	0.85	1.41	1.78	2.06	3.55	0.73	41.03	0.99

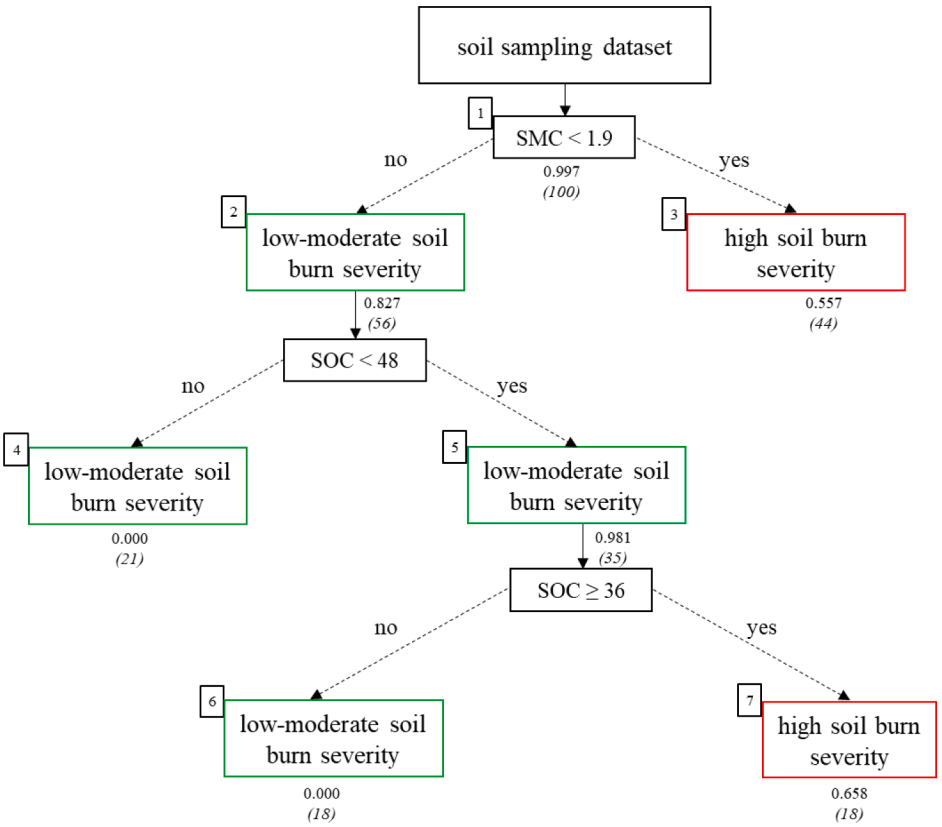

Fig. 6. Decision tree showing soil burn severity classified according to analyzed soil properties. We indicate the entropy value (without brackets) and the percentage of samples under the node (inside brackets).

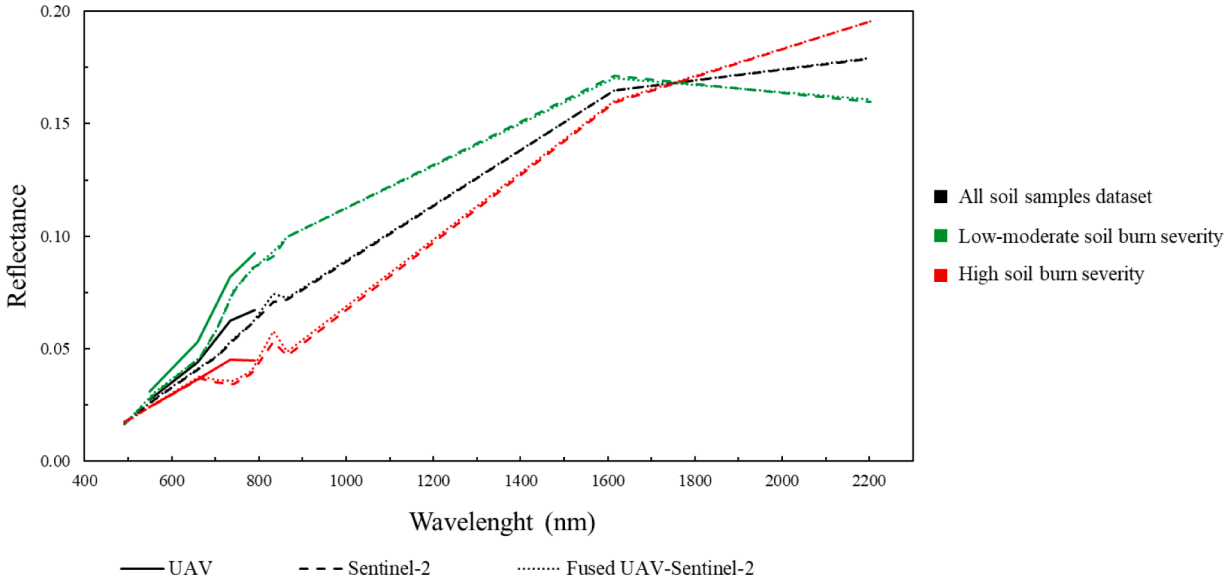

Fig. 7. Mean spectral reflectance of soil samples for the entire dataset and each soil burn severity category of all sensors used in this study, as well as their spatial and spectral fusion.

et al., 2019b; Fernández et al., 2021), can be attributed to the volatilization degree of organic matter in the most superficial soil layers as a function of the temperatures reached during the wildfire (Giovannini et al., 1988), and shows a large variability in mixed-severity wildfires, as found in northwest Spain by Vega et al. (2013).

Our results in burned areas mainly indicated that spatial resolution improvement of Sentinel-2 imagery with UAV data led to a significant increase in the accuracy of SOC prediction models, with a predictive capacity similar to that offered by laboratory VIS-NIR spectroscopy (Cañasveras et al., 2010; Debaene et al., 2014) or with hyperspectral spectrometer airborne imaging (Gomez et al., 2012). Even though the same modelling methods were applied to each dataset, the predictive performance was completely different when UAV and Sentinel-2 imagery were considered separately. The spectral richness of Sentinel-2

Table 4
Results derived from the leave-one-out cross-validation of the support vector machine (SVM) regression between the different spectral datasets and each soil property considered for the set of field plots located in the burned area affected.

Multispectral sensor type	Spatial resolution (m)	Soil organic carbon content SOC (µg C·g − 1 soil)				Soil moisture content SMC (%)			
		RMSE	RPD	RPIQ	R^2	RMSE	RPD	RPIQ	R^2
Sentinel-2A MSI	10	12.01	0.96	1.13	0.13	1.93	1.05	0.65	0.11
UAV Parrot Sequoia	0.50	10.03	1.14	1.35	0.24	2.04	0.99	0.65	0.01
Fused UAV-Sentinel-2	0.50	7.83	1.47	1.73	0.52	2.03	0.99	0.65	0.01

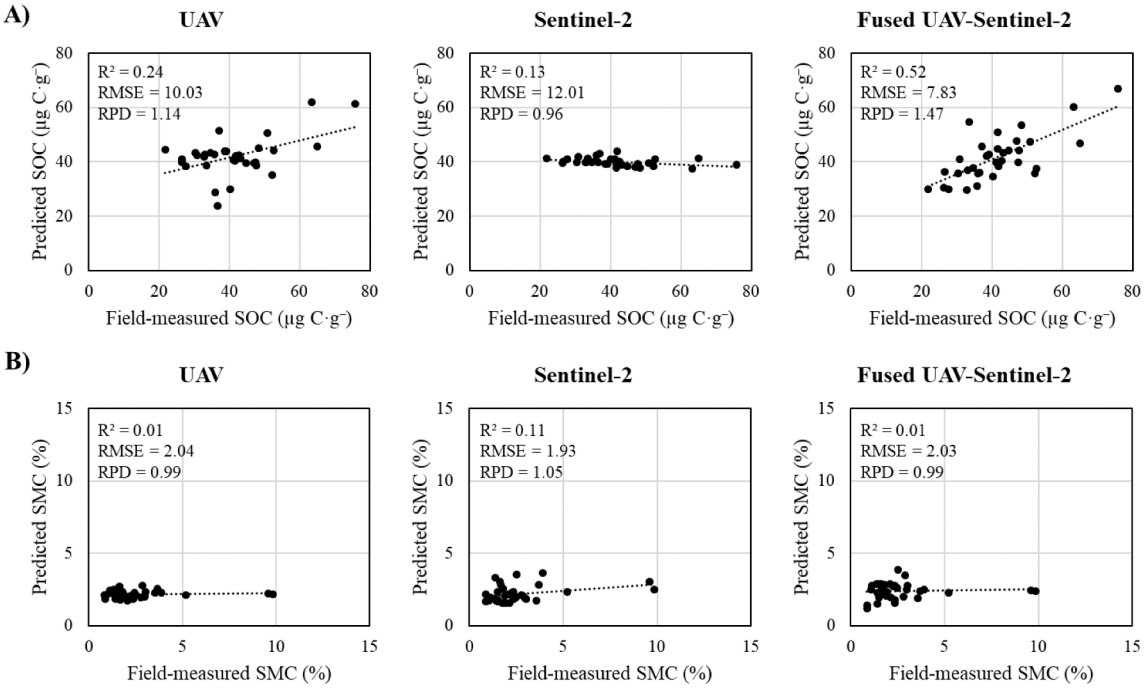

Fig. 8. Relationship through support vector machine (SVM) regression models between estimated values by each spectral dataset and field-measured values of (A) SOC and (B) SMC properties.

allows to properly discriminate SOC patches from the spectral composition and soil colouration. This is mainly due to the signal quality in the SWIR region which is related to organic matter compounds such as cellulose and lignin or starch, affecting the reflectance around 2100 nm and 2300 nm, respectively (Castaldi et al., 2016; Castaldi et al., 2019a). However, the degree of spatial agreement between Sentinel-2 pixels and real soil samples can negatively influence in SOC estimation (Lin et al., 2020). The high spatial variations in SOC content after fire showed their importance to enhanced the spatial resolution. The ground sample distance (GSD) of UAV allowed for greater detail of post-fire soil characteristics and textures, where the increase in ash or burned fine and coarse plant debris is closely related to SOC changes (Vega et al., 2013; Marcos et al., 2018). Therefore, fused image took advantage of the spatial quality of UAV image, achieving a better sharpness of the final product with a satisfactory ability to predict SOC content. Similar results were provided in other studies carried out in agricultural areas, where the high spatial and spectral resolution of fused images have proven to be useful in soil properties evaluation. For instance, Xu et al. (2018) observed positive correlations between soil total nitrogen and spectral indices based on visible and near-infrared bands derived from WorldView-2 (2 m of spatial resolution) and Landsat 8 OLI (30 m) fused images. In addition, the inclusion of spectrally and spatially enhanced remote sensing data significantly improved the accuracy of soil prediction maps in small and heterogeneous croplands (Xu et al., 2017). These further support statements promoting image fusion in soil investigation by exploiting the advantages of different sensor sources (Lin et al., 2020).

In agreement with Taktikou et al. (2016) and Adab et al. (2020), surface soil moisture prediction from passive remote sensing data remains a challenge. SMC is an essential soil variable after fire because affects water repellence in the first centimetres of the top soil (Arcenegui et al., 2008) and may influence surface runoff and erosion processes in the burned area (Badía et al., 2017). SMC was also able to discriminate soil burn severity, but it was poorly predicted from multispectral imagery. The higher spatial resolution offered by UAV and the fused UAV-Sentinel-2 image has not been effective enough in providing good relationships with the spatial distribution of soil water content. In burned areas, soil texture controls SMC spatial variability, although other factors such as slope, soil depth, soil surface or roughness also play a crucial role (Gómez-Plaza et al., 2000). Furthermore, the presence of a vegetation cover alters temporal patterns of moisture behaviour, showing a smaller effect in severely burned areas (higher temporal stability) than in slightly burned or unburned areas (Gómez-Plaza et al., 2000). The temporal changes have also hampered SMC determination despite optimal relationships between soil water content and SWIR reflectance from high spectral information imagery (Baroni et al., 2013; Taktikou et al., 2016). This spatial and temporal variability makes SMC a complex soil parameter to estimate by means of passive remote sensing techniques, as other authors have already shown (Gómez-Plaza et al., 2000; Baroni et al., 2013). In this regard, the physical sense of active remote sensing techniques such as synthetic-aperture radar (SAR) may be a more reliable alternative for SMC estimation (Kasischke et al., 2007). In addition, multi-temporal observations from large coverage satellite sensors have improved soil moisture modelling by resolving daily and

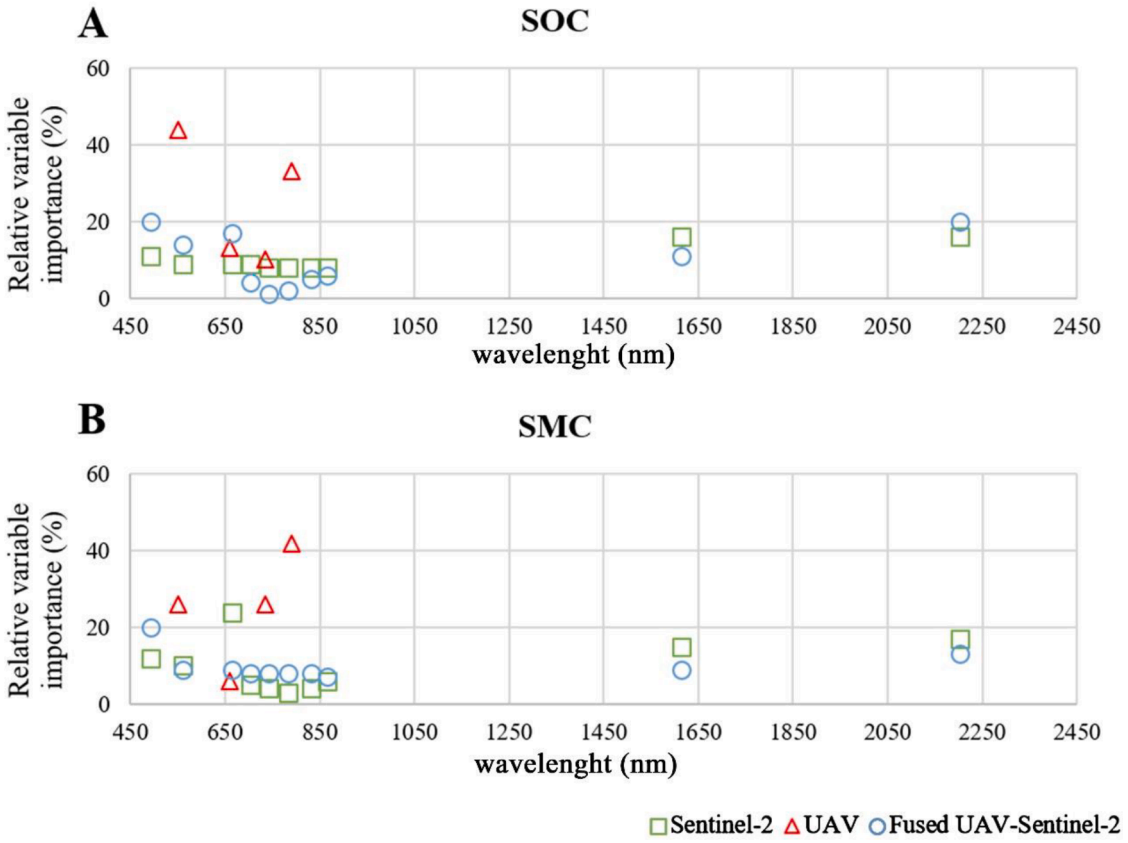

Fig. 9. Relative importance of the variables (reflectance bands) included in different regression models based on UAV, Sentinel-2 and fused UAV-Sentinel-2 datasets for the estimation of (A) SOC and (B) SMC.

seasonal distortions.

The spectral signatures indicated that the Gram-Schmidt (GS) transformation may correctly preserve the input spectral information in the fused image. Moreover, ERGAS index reflected the quality of the fused image in terms of normalized mean error of each processed band. The low ERGAS value indicated low distortion in the fused image, so the GS algorithm provides an optimal spectral-spatial performance commitment at these scales (Yilmaz and Gungor, 2016). This image sharpening technique has allowed us to incorporate accurate spatial information into the original multispectral image from Sentinel-2 and has also maintained the mean spectral response of each band in the fused image (Fig. 7). In accordance with previous studies in agricultural sites (Castaldi et al., 2016; Gholizadeh et al., 2018), the visible and SWIR were the most important regions for estimating soil properties through the fused image, mainly to SOC content. At these wavelengths, the reflectance response is strongly related to soil organic matter and water content, as well as other intrinsic soil factors such as particle size distribution, mineral composition, surface roughness, and colour of soil elements (Muller and Décamps, 2001). The lower relative importance of the NIR region in Sentinel-2 and in the fused UAV-Sentinel-2 images may be related to variations in the performance of the atmospheric correction methods employed in the pre-processed Sentinel-2 scene, as has been found with other satellite imagery (Vaudour et al., 2014). For example, overestimates in the B8A band have been observed in previous studies (Sola et al., 2018). Conversely, the reflectance from green and NIR bands of the Parrot Sequoia sensor on-board the UAV were the most important in the models. These bands have already proven to be useful for computing spectral indices related to soil burn severity (Beltrán-Marcos et al., 2021). However, in this study, we have further evidenced that the prediction of the spatial variability in soil burn severity through spectral indices was improved by using fused UAV-Sentinel-2 datasets because of the higher spatial/spectral information provided. In further research, the high spectral resolution of hyperspectral data together with high spatial resolution UAV data could allow a better discrimination of SOC content and other fire-sensitive soil properties in burned landscapes.

Although we reported promising findings in this study, some limitations should be highlighted. Jenerowicz and Woroszkiewicz (2016) noticed that the improvement of spatial resolution of multispectral image could imply a slight worsening of the spectral quality in the fused image. The low performance achieved in the SMC predictions could be due to underlying spatial variations in pre-fire soil characteristics in this specific study area, although alterations in spectral information could represent a potential supply of uncertainty. Logistic restraints in field sampling (e.g. a short period for data acquisition after the fire and specific distribution of soil field samples) could affect the generalization of the results. The requirement of adjusting the number and size of samples plots at the spatial resolution of Sentinel-2, and looking for homogeneous burned areas where tree canopy could not cause interference in the UAV data acquisition, may limit the representativeness and inference of the results. However, it has been shown that at small spatial scales, a small field dataset can be used to predict soil properties such as SOC, obtaining satisfactory results (Gomez et al., 2012; Debaene et al., 2014). Our results can be improved by using commercial satellite sensors with a higher spatial and spectral resolution (e.g. Worldview-2) (Yilmaz and Gungor, 2016; Xu et al., 2017) or aerial hyperspectral surveys (Ge et al., 2019). Moreover, further progress in increasing the predictive power of the fused datasets is needed. Nonetheless, the main advantage of the multispectral data used in this experimental work is that they can be obtained relatively cheaply and are almost immediately available. Therefore, they offer a cost-effective and reliable data source for mapping post-fire effects (Fernández-Guisuraga et al., 2018). High spatial resolution images from UAV platforms for soil burn severity estimation at the plot scale and Sentinel-2 data at the regional scale may

represent excellent support to forest management evaluations to identify priority areas where restoration post-fire actions need to be applied. The observation of spatial changes in SOC through novel remote sensing techniques such as image fusion contributes to advancing knowledge in severely damaged soils, allowing to act in areas with the greatest fire impact.

5. Conclusion

This pioneering study presents relevant results in the analysis of soil biophysical properties in burned areas by means the application of remote sensing image fusion techniques useful to predict the impact of fire at a very detailed spatial scale. Soil organic carbon (SOC) and soil moisture content (SMC) have been demonstrated to be good indicators of soil burn severity. The fusion of multispectral data at different spatial and spectral resolutions, collected immediately after wildfire by sensors on board a UAV and Sentinel-2A satellite platforms, provide a powerful tool to estimate soil organic carbon in complex and heterogeneous forest landscapes affected by mixed-severity fires. The image sharpening techniques of this study preserved the spectral information of satellite images with the addition of a very high spatial resolution particularly useful to characterize fire effects on soil. Nevertheless, more research is needed to explore further the effects of image sharpening on fire-sensitive soil properties prediction models.

Declaration of Competing Interest

The authors declare that they have no known competing financial interests or personal relationships that could have appeared to influence the work reported in this paper.

Data availability

Data will be made available on request.

Acknowledgments

This study was supported by the Spanish Ministry of Economy and Competitiveness and the European Regional Development Fund (ERDF) in the framework of the FIRESEVES project (AGL2017-86075-C2-1-R); by the Regional Government of the Principality of Asturias and Foundation for the Promotion of Applied Scientific Research and Technology in Asturias (FICYT) in the framework of the REWLDING project (AYUD/2021/51261); by the Regional Government of Castile and León in the framework of the WUIFIRECYL project (LE005P20); and by the Portuguese Foundation for Science and Technology in the frame of project UIDB/04033/2020. David Beltrán Marcos was supported by a predoctoral contract from the Regional Government of Castile and León co-financed by the European Social Fund (EDU/ 556/2019). José Manuel Fernández-Guisuraga was supported by a Ramón Areces Foundation postdoctoral fellowship.

Appendix A. Supplementary data

Supplementary data to this article can be found online at https://doi.org/10.1016/j.geoderma.2022.116290.

References

Adab, H., Morbidelli, R., Saltalippi, C., Moradian, M., Ghalhari, G.A.F., 2020. Machine learning to estimate surface soil moisture from remote sensing data. Water 12, 3223. https://doi.org/10.3390/W12113223.

Alcañiz, M., Outeiro, L., Francos, M., Úbeda, X., 2018. Effects of prescribed fires on soil properties: a review. Sci. Total Environ. 613, 944–957. https://doi.org/10.1016/j.scitotenv.2017.09.144.

Aldana-Jague, E., Heckrath, G., Macdonald, A., van Wesemael, B., Van Oost, K., 2016. UAS-based soil carbon mapping using VIS-NIR (480–1000 nm) multi-spectral imaging: Potential and limitations. Geoderma 275, 55–66. https://doi.org/10.1016/j.geoderma.2016.04.012.

Alparone, L., Wald, L., Chanussot, J., Thomas, C., Gamba, P., Bruce, L.M., 2007. Comparison of pansharpening algorithms: Outcome of the 2006 GRS-S data-fusion contest. IEEE Trans. Geosci. Remote Sens. 45, 3012–3021. https://doi.org/10.1109/TGRS.2007.904923.

Arcenegui, V., Mataix-Solera, J., Guerrero, C., Zornoza, R., Mataix-Beneyto, J., García-Orenes, F., 2008. Immediate effects of wildfires on water repellency and aggregate stability in Mediterranean calcareous soils. Catena 74, 219–226. https://doi.org/10.1016/j.catena.2007.12.008.

Badía, D., López-García, S., Martí, C., Ortíz-Perpiñá, O., Girona-García, A., Casanova-Gascón, J., 2017. Burn effects on soil properties associated to heat transfer under contrasting moisture content. Sci. Total Environ. 601, 1119–1128. https://doi.org/10.1016/j.scitotenv.2017.05.254.

Baroni, G., Ortuani, B., Facchi, A., Gandolfi, C., 2013. The role of vegetation and soil properties on the spatio-temporal variability of the surface soil moisture in a maize-cropped field. J. Hydrol. 489, 148–159. https://doi.org/10.1016/j.jhydrol.2013.03.007.

Beltrán-Marcos, D., Suárez-Seoane, S., Fernández-Guisuraga, J.M., Fernández-García, V., Pinto, R., García-Llamas, P., Calvo, L., 2021. Mapping soil burn severity at very high spatial resolution from unmanned aerial vehicles. Forests 12, 1–15. https://doi.org/10.3390/f12020179.

Breiman, L., Friedman, J.H., Olshen, R.A., Stone, C.J., 2017. Classification and regression trees. Classif. Regres. Trees 1–358. https://doi.org/10.1201/9781315139470/CLASSIFICATION-REGRESSION-TREES-LEO-BREIMAN-JEROME-FRIEDMAN-RICHARD-OLSHEN-CHARLES-STONE.

Calvo, L., Huerta, S., Marcos, E., Calvo-Fernández, J., Taboada, A., 2015. The role of prescribed fire in the provision of regulating ecosystem services of Spanish heathlands. Ecol. Quest. 21, 71–73. https://doi.org/10.12775/EQ.2015.012.

Cañasveras, J.C., Barrón, V., del Campillo, M.C., Torrent, J., Gómez, J.A., 2010. Estimation of aggregate stability indices in Mediterranean soils by diffuse reflectance spectroscopy. Geoderma 158, 78–84. https://doi.org/10.1016/J.GEODERMA.2009.09.004.

Castaldi, F., Chabrillat, S., Don, A., van Wesemael, B., 2019a. Soil Organic Carbon Mapping Using LUCAS Topsoil Database and Sentinel-2 Data: An Approach to Reduce Soil Moisture and Crop Residue Effects. Remote Sens. 2019, Vol. 11, Page 2121 11, 2121. https://doi.org/10.3390/RS11182121.

Castaldi, F., Palombo, A., Santini, F., Pascucci, S., Pignatti, S., Casa, R., 2016. Evaluation of the potential of the current and forthcoming multispectral and hyperspectral imagers to estimate soil texture and organic carbon. Remote Sens. Environ. 179, 54–65. https://doi.org/10.1016/j.rse.2016.03.025.

Castaldi, F., Hueni, A., Chabrillat, S., Ward, K., Buttafuoco, G., Bomans, B., Vreys, K., Brell, M., van Wesemael, B., 2019b. Evaluating the capability of the Sentinel 2 data for soil organic carbon prediction in croplands. ISPRS J. Photogramm. Remote Sens. 147, 267–282. https://doi.org/10.1016/j.isprsjprs.2018.11.026.

Cheng, K., Lu, Z., Zhou, Y., Shi, Y., Wei, Y., 2017. Global sensitivity analysis using support vector regression. Appl. Math. Model. 49, 587–598. https://doi.org/10.1016/J.APM.2017.05.026.

Collins, B.M., Kelly, M., Van Wagtendonk, J.W., Stephens, S.L., 2007. Spatial patterns of large natural fires in Sierra Nevada wilderness areas. Landsc. Ecol. 22, 545–557. https://doi.org/10.1007/S10980-006-9047-5/FIGURES/.

Cortez, P., 2020. Package 'rminer'. Data Mining Classification and Regression Methods. Version, R Package Version 1.4.6. 2020. Available online: https://cran.rproject.org/package=rminer http://www3.dsi.uminho.pt/pcortez/rminer.html (accessed on 6 May 2021).

Crucil, G., Castaldi, F., Aldana-Jague, E., van Wesemael, B., Macdonald, A., Van Oost, K., 2019. Assessing the performance of UAS-Compatible multispectral and hyperspectral sensors for soil organic carbon prediction. Sustainability 11 (7), 1889.

De'ath, G., Fabricius, K.E., 2000. Classification and regression trees: a powerful yet simple technique for ecological data analysis. Ecology 81, 3178–3192. https://doi.org/10.1890/0012-9658.

Debaene, G., Niedźwiecki, J., Pecio, A., Zurek, A., 2014. Effect of the number of calibration samples on the prediction of several soil properties at the farm-scale. Geoderma 214–215, 114–125. https://doi.org/10.1016/J.GEODERMA.2013.09.022.

Dragozi, E., Gitas, I.Z., Stavrakoudis, D.G., Theocharis, J.B., 2014. Burned area mapping using support vector machines and the FuzCoC feature selection method on VHR IKONOS imagery. Remote Sens. 6, 12005–12036. https://doi.org/10.3390/rs61212005.

Ehlers, M., 2004. Spectral characteristics preserving image fusion based on Fourier domain filtering. Remote Sens. Environ. Monit. GIS Appl. Geol. IV. 5574, 1. https://doi.org/10.1117/12.565160.

Ehlers, M., Klonus, S., Johan Åstrand, P., Rosso, P., 2010. Multi-sensor image fusion for pansharpening in remote sensing. Int. J. Image Data Fusion 1, 25–45. https://doi.org/10.1080/19479830903561985.

ESA, 2018. ESA: Level 2A input output data definition. Available online: http://step.esa.int/thirdparties/sen2cor/2.5.5/docs/S2-PDGS-MPC-L2A-IODD-V2.5.5.pdf (accessed on 8 April 2021).

ESA, 2021. Sentinel-2 User Guides. Available online: https://sentinel.esa.int/web/sentinel/user-guides/sentinel-2-msi/resolutions/radiometric (accessed on 8 April 2021).

Fernández, C., Fernández-Alonso, J.M., Vega, J.A., Fontúrbel, T., Llorens, R., Sobrino, J. A., 2021. Exploring the use of spectral indices to assess alterations in soil properties in pine stands affected by crown fire in Spain. Fire Ecol. 17, 1–11. https://doi.org/10.1186/s42408-020-00089-7.

Fernández-García, V., Marcos, E., Fernández-Guisuraga, J.M., Taboada, A., Suárez-Seoane, S., Calvo, L., 2019a. Impact of burn severity on soil properties in a *Pinus pinaster* ecosystem immediately after fire. Int. J. Wildl. Fire 28, 354–364. https://doi.org/10.1071/WF18103.

Fernández-García, V., Miesel, J., Baeza, M.J., Marcos, E., Calvo, L., 2019b. Wildfire effects on soil properties in fire-prone pine ecosystems: Indicators of burn severity legacy over the medium term after fire. Appl. Soil Ecol. 135, 147–156. https://doi.org/10.1016/j.apsoil.2018.12.002.

Fernández-Guisuraga, J.M., Sanz-Ablanedo, E., Suárez-Seoane, S., Calvo, L., 2018. Using unmanned aerial vehicles in postfire vegetation survey campaigns through large and heterogeneous areas: opportunities and challenges. Sensors 18, 586. https://doi.org/10.3390/s18020586.

Ge, Y., Thomasson, J.A., Sui, R., 2011. Remote sensing of soil properties in precision agriculture: a review. Front. Earth Sci. 5, 229–238. https://doi.org/10.1007/s11707-011-0175-0.

Ge, X., Wang, J., Ding, J., Cao, X., Zhang, Z., Liu, J., Li, X., 2019. Combining UAV-based hyperspectral imagery and machine learning algorithms for soil moisture content monitoring. PeerJ. 7, e6926.

Genuer, R., Poggi, J.M., Tuleau-Malot, C., 2010. Variable selection using random forests. Pattern Recognit. Lett. 31, 2225–2236. https://doi.org/10.1016/J.PATREC.2010.03.014.

GEODE., 2019. Mapa Geológico Digital Continuo de España. Scale 1:50000. Sheets 230 and 231; Ministerio de Industria y Energía: Madrid, Spain, 1982. Available online: http://mapas.igme.es/gis/rest/services/Cartografia_Geologica/IGME_Geode_50/MapServer (accessed on 18 March 2020).

Gholizadeh, A., Žižala, D., Saberioon, M., Borůvka, L., 2018. Soil organic carbon and texture retrieving and mapping using proximal, airborne and Sentinel-2 spectral imaging. Remote Sens. 218, 89–103. https://doi.org/10.1016/j.rse.2018.09.015.

Giovannini, G., Lucchesi, S., Giachetti, M., 1988. Effect of heating on some physical and chemical parameters related to soil aggregation and erodibility. Soil Sci. 146, 255–261. https://doi.org/10.1097/00010694-198810000-00006.

Gomez, C., Lagacherie, P., Coulouma, G., 2012. Regional predictions of eight common soil properties and their spatial structures from hyperspectral Vis–NIR data. Geoderma 189–190, 176–185. https://doi.org/10.1016/J.GEODERMA.2012.05.023.

Gómez-Plaza, A., Alvarez-Rogel, J., Albaladejo, J., Castillo, V.M., 2000. Spatial patterns and temporal stability of soil moisture across a range of scales in a semi-arid environment. Hydrol. Process. 14, 1261–1277. https://doi.org/10.1002/(sici)1099-1085(200005)14:7<1261::aid-hyp40>3.3.co;2-4.

ITACYL., 2020. Instituto Tecnológico y Agrario de Castilla y León (ITACYL). Portal de suelos. Visor de Datos de Suelos. Available online: http://suelos.itacyl.es/visor_datos.

Jenerowicz, A., Woroszkiewicz, M., 2016. The pan-sharpening of satellite and UAV imagery for agricultural applications. In: Remote Sensing for Agriculture, Ecosystems, and Hydrology XVIII. N, C.M.U., M, A., (Eds.)., Spie-Int Soc Optical Engineering, Bellingham, DC. 9998. https://doi.org/10.1117/12.2241645.

Jia, K., Liang, S., Gu, X., Baret, F., Wei, X., Wang, X., Yao, Y., Yang, L., Li, Y., 2016. Fractional vegetation cover estimation algorithm for Chinese GF-1 wide field view data. Remote Sens. Environ. 177, 184–191. https://doi.org/10.1016/j.rse.2016.02.019.

Johnstone, J.F., Chapin, F.S., 2006. Effects of soil burn severity on post-fire tree recruitment in boreal forest. Ecosystems 9, 14–31. https://doi.org/10.1007/S10021-004-0042-X/FIGURES/10.

Jones, A., Montanarella, L., Jones, R., 2005. In: Soil Atlas of Europe. European Commission, Luxembourg, pp. 64–65.

Jones, E.G., Wong, S., Milton, A., Sclauzero, J., Whittenbury, H., McDonnell, M.D., 2020. The impact of pan-sharpening and spectral resolution on vineyard segmentation through machine learning. Remote Sens. 12, 934. https://doi.org/10.3390/rs12060934.

Kaplan, G., 2018. Sentinel-2 Pan Sharpening—Comparative Analysis. Multidiscipl. Dig. Publ. Inst. Proc. 2, 345. https://doi.org/10.3390/ecrs-2-05158.

Kasischke, E.S., Bourgeau-Chavez, L.L., Johnstone, J.F., 2007. Assessing spatial and temporal variations in surface soil moisture in fire-disturbed black spruce forests in Interior Alaska using spaceborne synthetic aperture radar imagery — Implications for post-fire tree recruitment. Remote Sens. Environ. 108, 42–58. https://doi.org/10.1016/J.RSE.2006.10.020.

Keeley, J.E., 2009. Fire intensity, fire severity and burn severity: a brief review and suggested usage. Int. J. Wildl. Fire. 18, 116. https://doi.org/10.1071/WF07049.

Kemper, W.D., Rosenau, R.C., 1986. Aggregate stability and size distribution. Methods of soil analysis: Part 1. Phys. Mineral. Methods 9, 425–442.

Key, C. H., Benson, N. C., 2006. Landscape assessment: ground measure of severity, the composite burn index; and remote sensing of severity, the normalized burn ratio. In: Lutes, D.C., Keane, R.E., Caratti, J.F., Key, C.H., Benson, N.C., Sutherland, S., Gangi, L.J. (Eds.), FIREMON: Fire Effects Monitoring and Inventory System. USDA Forest Service, Rocky Mountain Research Station, Ogden, UT, pp. 1–51 Gen. Tech. Rep. RMRSGTR- 164-CD: LA.

Kisi, O., Parmar, K.S., 2016. Application of least square support vector machine and multivariate adaptive regression spline models in long term prediction of river water pollution. J. Hydrol. 534, 104–112. https://doi.org/10.1016/J.JHYDROL.2015.12.014.

Kuhn, M., 2008. Building predictive models in R using the caret package. J Stat Softw, 28, 1-26. Available online: http://topepo.github.io/caret/index.html (accesed on 6 May 2021).

Laben, C., Brower, B., 2000. Process for enhancing the spatial resolution of multispectral imagery using pan-sharpening. United States Patent 6, 11, 875.

Lentile, L.B., Holden, Z.A., Smith, A.M.S., Falkowski, M.J., Hudak, A.T., Morgan, P., Lewis, S.A., Gessler, P.E., Benson, N.C., 2006. Remote sensing techniques to assess active fire characteristics and post-fire effects. Int. J. Wildl. Fire. 15, 319–345. https://doi.org/10.1071/WF05097.

Lin, C., Zhu, A.X., Wang, Z., Wang, X., Ma, R., 2020. The refined spatiotemporal representation of soil organic matter based on remote images fusion of Sentinel-2 and Sentinel-3. Int. J. Appl. Earth Obs. Geoinf. 89, 102094 https://doi.org/10.1016/J.JAG.2020.102094.

Lu, P., Wang, L., Niu, Z., Li, L., Zhang, W., 2013. Prediction of soil properties using laboratory VIS–NIR spectroscopy and Hyperion imagery. J. Geochemical Explor. 132, 26–33. https://doi.org/10.1016/J.GEXPLO.2013.04.003.

Marcos, E., Tárrega, R., Calvo, L., Luis-Calabuig, E. 2009. Efectos del fuego sobre el suelo bajo comunidades arbustivas y arbóreas de la provincia de León. Los brezales como caso de estudio. In: Cerdá, A., Mataix-Solera, J (Eds.). Efecto de los incendios forestales sobre los suelos en España. El estado de la cuestión visto por los científicos españoles. Cátedra de Divulgación de la Ciencia. Universitat de Valencia. pp. 133-155.

Marcos, E., Fernández-García, V., Fernández-Manso, A., Quintano, C., Valbuena, L., Tárrega, R., Luis-Calabuig, E., Calvo, L., 2018. Evaluation of composite burn index and land surface temperature for assessing soil burn severity in mediterranean fire-prone pine ecosystems. Forests 9, 1–16. https://doi.org/10.3390/f9080494.

Mataix-Solera, J., Gómez, I., Navarro-Pedreño, J., Guerrero, C., Moral, R., 2002. Soil organic matter and aggregates affected by wildfire in a *Pinus halepensis* forest in a Mediterranean environment. Int. J. Wildl. Fire 11, 107–114. https://doi.org/10.1071/WF02020.

Mataix-Solera, J., Cerdà, A., Arcenegui, V., Jordán, A., Zavala, L.M., 2011. Fire effects on soil aggregation: a review. Earth-Sci. Rev. 109, 44–60. https://doi.org/10.1016/j.earscirev.2011.08.002.

Maurer, T., 2013. How to pan-sharpen images using the gram-schmidt pan-sharpen method–A recipe. Int. Arch. Phhotogrammetry Remote Sens. Spatial Infor. Sci. 1, W1.

Meyer, D., Dimitriadou, E., Hornik, K., Weingessel, A., Leisch, F., 2015. e1071: Misc functions of the department of statistics, probability theory group (formerly: E1071), TU Wien. R package version 1. 6–7 (http://CRAN.R-project.org/package=e1071).

Miller, J.D., Thode, A.E., 2007. Quantifying burn severity in a heterogeneous landscape with a relative version of the delta Normalized Burn Ratio (dNBR). Remote Sens. Environ. 109, 66–80. https://doi.org/10.1016/j.rse.2006.12.006.

Moreira, F., Viedma, O., Arianoutsou, M., Curt, T., Koutsias, N., Rigolot, E., Barbati, A., Corona, P., Vaz, P., Xanthopoulos, G., Mouillot, F., Bilgili, E., 2011. Landscape - wildfire interactions in southern Europe: Implications for landscape management. J. Environ. Manage. 92, 2389–2402. https://doi.org/10.1016/j.jenvman.2011.06.028.

Morgan, P., Hardy, C.C., Swetnam, T.W., Rollins, M.G., Long, D.G., 2001. Mapping fire regimes across time and space: understanding coarse and fine-scale fire patterns. Int. J. Wildl. Fire. 10, 329–342. https://doi.org/10.1071/wf01032.

Muller, E., Décamps, H., 2001. Modeling soil moisture–reflectance. Remote Sens. Environ. 76, 173–180. https://doi.org/10.1016/S0034-4257(00)00198-X.

Neary, D. G., Ryan, K. C., DeBano, L. F., 2005. Wildland fire in ecosystems: effects of fire on soils and water. In Gen. Tech. Rep. RMRS-GTR-42. USDA Forest Service, Rocky Mountain Research Station, Fort Collins CO, 250. https://doi.org/10.2737/RMRS-GTR-42-V4.

Nelson, D.W., Sommers, L.E., 1982. Total carbon, organic carbon and organic matter. In: Klute, A. (Ed.), Methods of Soil Analysis, Part 2: Chemical and Microbiological Properties. ASA, Madison, Wisconsin, USA, pp. 539–579.

Ninyerola, M., Pons, X., Roure, J.M., 2005. Atlas Climático Digital de la Península Ibérica. Universidad Autónoma de Barcelona, Metodología y aplicaciones en bioclimatología y geobotánica.

Parks, S., Dillon, G., Miller, C., 2014. A New Metric for Quantifying Burn Severity: The Relativized Burn Ratio. Remote Sens. 6, 1827–1844. https://doi.org/10.3390/rs6031827.

Pausas, J.G., Fernández-Muñoz, S., 2012. Fire regime changes in the Western Mediterranean Basin: from fuel-limited to drought-driven fire regime. Clim. Change 110, 215–226. https://doi.org/10.1007/s10584-011-0060-6.

Pausas, J.G., Llovet, J., Rodrigo, A., Vallejo, R., 2008. Are wildfires a disaster in the Mediterranean basin? A review. Int. J. Wildl. Fire 17, 713–723. https://doi.org/10.1071/WF07151.

Pereira, P., Francos, M., Brevik, E.C., Ubeda, X., Bogunovic, I., 2018. Post-fire soil management. Curr. Opin. Environ. Sci. Heal. 5, 26–32. https://doi.org/10.1016/j.coesh.2018.04.002.

Puliti, S., Ørka, H., Gobakken, T., Næsset, E., 2015. Inventory of small forest areas using an unmanned aerial system. Remote Sens. 7, 9632–9654. https://doi.org/10.3390/rs70809632.

Quintano, C., Fernández-Manso, A., Calvo, L., Marcos, E., Valbuena, L., 2015. Land surface temperature as potential indicator of burn severity in forest Mediterranean ecosystems. Int. J. Appl. Earth Obs. Geoinf. 36, 1–12. https://doi.org/10.1016/j.jag.2014.10.015.

Ripley, B. 2019. Package 'tree'. Classification and Regression Trees. Version, R Package Version 1.0-40. 2019. Available online: https://CRAN.R-project.org/package=tree (accessed on 6 May 2021).

Ripley, T., Atkinson, B., Ripley, B. 2022. Package "rpart". Recursive partitioning for classification, regression and survival trees. An implementation of most of the functionality of the 1984 book by Breiman, Friedman, Olshen and Stone. https://cran.r-project.org/web/packages/rpart/index.html (accessed on 5.April.2022).

R Core Team, 2019. R: A language and environment for statistical computing. R Foundation for Statistical Computing, Vienna, Austria. https://www.R-project.org/. Accessed 03 March 2021.

Rivera, J., Verrelst, J., Leonenko, G., Moreno, J., 2013. Multiple cost functions and regularization options for improved retrieval of leaf chlorophyll content and LAI through inversion of the PROSAIL Model. Remote Sens. 5, 3280–3304. https://doi.org/10.3390/rs5073280.

Ruzgiene, B., Berteška, T., Gečyte, S., Jakubauskiene, E., Aksamitauskas, V.Č., 2015. The surface modelling based on UAV Photogrammetry and qualitative estimation. Meas. J. Int. Meas. Confed. 73, 619–627. https://doi.org/10.1016/j.measurement.2015.04.018.

Sherrod, P.H., 2008. DTREG Predictive Modeling Software. Users Manual. www.dtreg.com/DTREG.pdf.

Shi, P., Castaldi, F., van Wesemael, B., Van Oost, K., 2020. Vis-NIR spectroscopic assessment of soil aggregate stability and aggregate size distribution in the Belgian Loam Belt. Geoderma 357, 113958. https://doi.org/10.1016/J.GEODERMA.2019.113958.

Sola, I., García-Martín, A., Sandonís-Pozo, L., Álvarez-Mozos, J., Pérez-Cabello, F., González-Audícana, M., Montorio-Llovería, R., 2018. Assessment of atmospheric correction methods for Sentinel-2 images in Mediterranean landscapes. International Journal of Applied Earth Observation and Geoinformation 73, 63–76. https://doi.org/10.1016/j.jag.2018.05.020.

Soriano-Disla, J.M., Janik, L.J., Allen, D.J., McLaughlin, M.J., 2017. Evaluation of the performance of portable visible-infrared instruments for the prediction of soil properties. Biosyst. Eng. 161, 24–36. https://doi.org/10.1016/j.biosystemseng.2017.06.017.

Stevens, A., Miralles, I., van Wesemael, B., 2012. Soil organic carbon predictions by airborne imaging spectroscopy: comparing cross-validation and validation. Soil Sci. Soc. Am. J. 76, 2174–2183. https://doi.org/10.2136/sssaj2012.0054.

Taktikou, E., Bourazanis, G., Papaioannou, G., Kerkides, P., 2016. Prediction of soil moisture from remote sensing data. Procedia Eng. 162, 309–316. https://doi.org/10.1016/j.proeng.2016.11.066.

Tehrany, M.S., Pradhan, B., Jebur, M.N., 2013. Spatial prediction of flood susceptible areas using rule based decision tree (DT) and a novel ensemble bivariate and multivariate statistical models in GIS. J. Hydrol. 504, 69–79. https://doi.org/10.1016/j.jhydrol.2013.09.034.

Vaiopoulos, A.D., Karantzalos, K., 2016. Pansharpening on the narrow VNIR and SWIR spectral bands of Sentinel-2 ISPRS-Int. Arch. Photogram.,. Remote Sens. Spatial Inform. Sci. XLI-B7 41, 723–730. https://doi.org/10.5194/isprsarchives-XLI-B7-723-2016.

Van Der Werf, G.R., Randerson, J.T., Giglio, L., Collatz, G.J., Mu, M., Kasibhatla, P.S., Morton, D.C., Defries, R.S., Jin, Y., Van Leeuwen, T.T., 2010. Global fire emissions and the contribution of deforestation, savanna, forest, agricultural, and peat fires (1997–2009). Atmos. Chem. Phys. 10, 11707–11735. https://doi.org/10.5194/acp-10-11707-2010.

Vapnik V., 1995. The Nature of Statistical Learning Theory. Wiley Press, New York, USA.

Vaudour, E., Gilliot, J.M., Bel, L., Bréchet, L., Hamiache, J., Hadjar, D., Lemonnier, Y., 2014. Uncertainty of soil reflectance retrieval from SPOT and RapidEye multispectral satellite images using a per-pixel bootstrapped empirical line atmospheric correction over an agricultural region. Int. J. Appl. Earth Obs. Geoinf. 26, 217–234. https://doi.org/10.1016/J.JAG.2013.07.003.

Vaudour, E., Gomez, C., Fouad, Y., Lagacherie, P., 2019. Sentinel-2 image capacities to predict common topsoil properties of temperate and Mediterranean agroecosystems. Remote Sens. Environ. 223, 21–33. https://doi.org/10.1016/J.RSE.2019.01.006.

Vega, J.A., Fontúrbel, T., Merino, A., Fernández, C., Ferreiro, A., Jiménez, E., 2013. Testing the ability of visual indicators of soil burn severity to reflect changes in soil chemical and microbial properties in pine forests and shrubland. Plant Soil. 369, 73–91. https://doi.org/10.1007/s11104-012-1532-9.

Venables, W.N., Ripley, B.D., 2002. Modern Applied Statistics Con S. Springer.

Vivone, G., Alparone, L., Chanussot, J., Dalla Mura, M., Garzelli, A., Licciardi, G.A., Restaino, R., Wald, L., 2015. A critical comparison among pansharpening algorithms. IEEE Trans. Geosci. Remote Sens. 53, 2565–2586. https://doi.org/10.1109/TGRS.2014.2361734.

Wald, L., Ranchin, T., Mangolini, M., 1997. Fusion of satellite images of different spatial resolutions: Assessing the quality of resulting images. Photogramm. Eng. Remote Sensing 63, 691–699.

Xu, Y., Smith, S.E., Grunwald, S., Abd-Elrahman, A., Wani, S.P., 2017. Incorporation of satellite remote sensing pan-sharpened imagery into digital soil prediction and mapping models to characterize soil property variability in small agricultural fields. ISPRS J. Photogramm. Remote Sens. 123, 1–19. https://doi.org/10.1016/j.isprsjprs.2016.11.001.

Xu, Y., Smith, S.E., Grunwald, S., Abd-Elrahman, A., Wani, S.P., 2018. Effects of image pansharpening on soil total nitrogen prediction models in South India. Geoderma 320, 52–66. https://doi.org/10.1016/j.geoderma.2018.01.017.

Yilmaz, V., Gungor, O., 2016. Fusion of very high-resolution UAV images with criteria-based image fusion algorithm. Arab. J. Geosci. 9, 1–16. https://doi.org/10.1007/s12517-015-2109-8.

Zhang, C., Kovacs, J.M., 2012. The application of small unmanned aerial systems for precision agriculture: a review. Precis. Agric. 13, 693–712. https://doi.org/10.1007/s11119-012-9274-5.

Zhang, Y., Mishra, R.K., 2012. A review and comparison of commercially available pan-sharpening techniques for high resolution satellite image fusion. Int. Geosci. Remote Sens. Symp. 182–185 https://doi.org/10.1109/IGARSS.2012.6351607.

Zhao, L., Shi, Y., Liu, B., Hovis, C., Duan, Y., Shi, Z., 2019. Finer classification of crops by fusing UAV images and sentinel-2A data. Remote Sens. 11, 3012. https://doi.org/10.3390/rs11243012.

Žížala, D., Minarík, R., Zádorová, T., 2019. Soil organic carbon mapping using multispectral remote sensing data: Prediction ability of data with different spatial and spectral resolutions. Remote Sens. 11, 1–23. https://doi.org/10.3390/rs11242947.